Review

Unexpected Ferromagnetism—A Review

Iulia Ioana Lungu [1,2,*], Alexandru Mihai Grumezescu [1,3,4] and Claudiu Fleaca [2]

1   Faculty of Applied Chemistry and Materials Science, University Politehnica of Bucharest,
    011061 Bucharest, Romania; grumezescu@yahoo.com
2   National Institute of Laser, Plasma and Radiation Physics (NILPRP), 077125 Magurele, Romania;
    claudiu.fleaca@inflpr.ro
3   Research Institute of the University of Bucharest—ICUB, University of Bucharest, 050657 Bucharest, Romania
4   Academy of Romanian Scientists, Ilfov No. 3, 50044 Bucharest, Romania
*   Correspondence: iulia.lunguu@gmail.com

Abstract: The study of magnetism in materials without partially filled d or f bands has gained much attention in the past years. Even though it has challenged the understanding of traditional magnetism, there is a wide range of studies debating the nature of magnetism in such materials. Theories on whether the exhibited ferromagnetic behavior is due to sample impurities or intrinsic structural defects have been published throughout the years. Materials such as hexaborides, non-magnetic oxides, and carbon nanostructures have been of great interest due to their potential applications. For a better understanding, herein, we present a literature review combining past and up-to-date studies on these materials.

Keywords: d^0 magnetism; room temperature ferromagnetism; alkaline-earth hexaborides; non-magnetic oxides; carbon nanostructures

1. Conventional vs. d^0 Magnetism

It is commonly known that, in order for a material to exhibit magnetic behavior, one of the most important requirements is to have partially filled d or f bands. The magnetic order is achieved by the exchange interactions among the above-mentioned partially filled bands. However, challenging to the common knowledge of how magnetism works, it has been discovered that some nanomaterials, with either entirely empty or full d and f bands, exhibit unexpected magnetic behavior. Unexpected magnetism can be induced by reducing one, or more, of the materials' dimensions. Reducing at least one dimension leads to the restriction in the electrons' tendency to "jump" from one atomic site to the other, also known as "electron hopping". Therefore, the kinetic energy of the electrons is diminished while increasing the ratio between the electrostatic interactions in electric charges and the kinetic energy (Coulomb interactions/bandwidth ratio); this enhances the possibility of reduced scale materials to exhibit magnetism [1].

Nanomagnetism is a field that studies the magnetic behavior of certain materials at a nanometric scale. Because of the increased surface-to-volume ratio, the magnetic features of nanomaterials can be fully contrasting from those of the bulk material, which have an identical chemical composition. Due to extensive research on the topic, the magnetic characteristics of bulk ferro- and antiferro-magnetic materials contrast with the corresponding material at the nanometer scale. Moreover, it has been observed that some nanomaterials may exhibit ferromagnetism at room temperature, in spite of the fact that the initial material is not magnetically active at all. There are several structural and geometrical features that control the magnetism behavior of a certain material: The distance between atoms, ligancy (coordination number), and symmetry. There are several consequences to modifying the structure of a nanomaterial. The modification of the local environment of the atoms can be attained through defect introduction, such as impurities, vacancies, and vacancy complexes. By reducing the ligancy and changing the symmetry, the energy level

bands are expected to narrow. This is the reason for the enhancement of magnetism in materials with ferromagnetic behavior; and could also explain why some non-magnetic materials exhibit magnetic behavior [2].

The main difference between non-magnetic and magnetic materials is that, for the first type, without the interference of an external magnetic field, the magnetization density is zero, whereas, for the latter, in the same conditions, the magnetization density is finite. Whereas the magnetic materials are attracted to an external magnetic field, many other materials are repelled by this kind of field, thus having a diamagnetic behavior. There are also paramagnetic materials that are weakly attracted by an external magnetic field, yet, unlike the ferromagnets, their magnetization vanishes when the field is removed due to the thermal motion, which causes random orientation of uncoupled spins. In order for an element to be in a ferromagnetic state, it has to have unpaired electrons and mechanisms that drive the ferromagnetic coupling of the mentioned unpaired electrons. However, even though the electrons of an atom have a magnetic field, this does not translate to the fact that the atom itself has a magnetic field. In order for this to happen, the unpaired electrons must be located in the outer shells. An example of an atom with a strong magnetic field is iron due to its four unpaired electrons found on the outer shell. However, even though the existence of unpaired electrons is necessary for ferromagnetism, it is not enough. The electrons found in higher orbitals have higher kinetic energy and, therefore, lower potential energy. This correlates to the need for unpaired electrons on low energy levels, meaning they are closer to the nucleus [2]. There are only three elements in the periodic table that exhibit ferromagnetism at room temperature, namely iron, cobalt, and nickel. d^0 magnetism is a term that has been used to describe materials that display room temperature ferromagnetism when they should not be ferromagnetic at all [1,2]. Some examples of this behavior have been found in hexaborides, non-magnetic oxides, and carbon structures, further discussed in the following sections, as well as exemplified in Table 1.

As resumed in [3], the appearance of ferromagnetism in various semiconductors or in some insulators doped with 3d ions occurs even if the concentration of these ions is much lower than the percolation required for their nearby coupling. In these materials, the mediated moment per cation is near or even greater than the moment induced by uncoupled spins in conditions where dopant concentrations were low, and this moment decreases as the concentration approaches towards those of percolation [3]. It was also highlighted that the magnetic properties show great variations for materials with the same apparent compositions synthesized by different researcher groups or by various methods [3].

Known for about three decades, non-oxidic diluted magnetic semiconductors (DMSs) with p-type electronic conduction are based on combinations between elements from main group III and V (such as GaAs, InAs, GaP, GaSb, GaN) and even from a single element from group IV such as Ge, all doped with Mn^{2+} ions [4]. For example, the materials from $Ga_{1-x}Mn_x$ as a system having x = 0.03 to 0.07 have a ferromagnetic (FM) behavior with a Curie temperature Tc ~ 100 K [5]. For this class of materials, the authors from [5] concluded that the apparition of a ferromagnetic phase when the temperature was sufficiently decreased was caused by the interaction between magnetic manganese ions induced by the charge carriers (in these cases being holes) in the host matrix. Thus, the exchange interaction of localized holes with magnetic dopants leads to the formation of so-called bound magnetic polarons (BMPs), which are composed of one localized hole (in the p valence band) and a considerable number of magnetic ions around it [5]. Even if the nearby spins of the magnetic impurities tend to align in the same direction and are in opposition with the hole spin, thus having a direct antiferromagnetic exchange interaction inside BMPs, there is a possibility of FM interaction between BMPs at a high concentration of magnetic dopants [5]. Moreover, when the temperature is sufficiently low, the BMPs tend to overlap while mutually interacting via nearby magnetic dopants. Consequently, the spins of polarons will align and thus, when interacting polarons clusters grow to the dimensions of all the material, it can be considered that a ferromagnetic transition occurred [5]. It

must be pointed out that, for this kind of DMSs (especially for the insulating ones), their observed saturation magnetization is much lower than a similar system with the ideal full ordering of magnetic dopants, which can be explained if a great fraction of magnetic dopants have a zero contribution the sample ferromagnetism [4]. Additionally, in the range of concentrations where DMS FM is observable, the magnetic ions are intercalated between non-magnetic atoms, so they are separated, thus any antiferromagnetic interactions between these ions can be neglected due to their rapid diminution with the increasing distance [4].

The BMPs approach was also used to explain FM in diluted magnetic oxides having an n-type conduction type [3]. In these cases, the introduction of a dopant magnetic cation (M) between the non-magnetic cations (A) and oxygen anions will induce the formation of a defect (D, named "donor defect") in the host lattice formulated now as [A1-xMx][ODδ]n (where δ is the donor concentration and x is 1 or 2 corresponding to divalent or tetravalent non-magnetic cations), a defect which is associated with an electron (similar situation with the hole in p-type DMSs) which was treated similarly with a 1s electron in a hydrogenoid atom, having a specific radius and mass [3]. The orbitals associated with these uncoupled electrons tend to overlap, forming a so-called "impurity band" when the concentration of donor defects increases. At low concentrations, these electrons are strictly localized due to their narrow band fluctuations of potential, whereas at higher concentrations, when they reach a critical donor concentration, these impurity states lose their localization which implies metallic-type conduction. Here the BMPs are formed by coupling the orbits of these hydrogenoid defect-bounded electrons with 3d moments of magnetic ion dopants [3]. Thus, when the radius of this hydrogenoid electron orbital is large enough, their overlapping with the nearby magnetic cations will induce the apparition of a FM exchange coupling which is also influenced by the spin of 3d cations. The calculation showed that in a sphere with the radius of a hydrogenoid 1s electron there can be from ~10 to ~100 cationic sites [3]. For example, in the case of the d5 cations such as Mn^{2+} or Fe^{3+}, the remaining unoccupied orbitals are available only for electrons with spin down. Because the donor electron will have also spin down ($\downarrow$), if the two magnetic impurities will fall in the same donor orbital due the parallel alignment of the spins, the resulting effective coupling will be ferromagnetic. The authors concluded that the coupling between the donor electron and the magnetic cation is ferromagnetic for the case when the 3d ionic shell is occupied less than half and antiferromagnetic if the 3d shell is half or over half occupied, whereas, for the case of two similar impurities interacting both within the same donor orbital, the coupling is ferromagnetic [3]. Additionally, the landscape of different magnetic interactions is shaped by both polaron and cation percolation threshold. If the number of cationic dopants sites within the sphere of hydrogenoid electron is high enough, the FM will occur when the concentration of donors is greater than those of donors percolations accompanied by a lower than specific percolation concentration of magnetic cations. Other behaviors, like antiferromagnetism or ferrimagnetism will manifest at concentrations exceeding those of magnetic cations percolation [3]. Regarding the Curie temperature (Tc) in these doped oxidic systems, it can be an estimated function of many parameters: J_{sd} (s-d exchange parameter), S (3d cation spins), s (donor electron spin), concentrations of cations (x), and donors (δ), ω_c (cation volume fraction, ε_F (Fermi energy in the impurity band) according to the Equation (1):

$$T_C = S(S + 1)s^2 nx\delta J_{sd}^2 \omega_c^{2/3} / k_B \varepsilon_F \qquad (1)$$

where k_B is Boltzmann constant [3] and even this expression is much simplified, given lower than real values of Tc.

The authors from [3] suggest that, for the cases where the donors' concentrations are sufficiently high, the model involving the impurity band does not apply anymore, due to the fact that the energy of the donor state is merging with the inferior part of the conduction band and here the RKKKY (Ruderman–Kittel–Kasuya–Yosida) exchange is applicable. If the separation between nearby magnetic cations is smaller than the localization length, the RKKY interaction will work even if the mobility edge is above the Fermi level. Thus, the

Fermi wavevector noted KF has a small value on the base of the band, translated in the fact that, at low electron densities, the RKKKY exchange interactions will be of FM type. However, at higher electron density, the system will behave like a spin glass due to the fact that the exchange of positive and negative bonds of the equal number will cancel each other [3].

One main type of defect which gives rise to the donors is considered to be the oxygen vacancies in n-type oxides. Whereas in the two-electron occupied vacancy (F0 centers) the 1s2 state is usually in a singlet state and is responsible only for weak antiferromagnetic exchange, the one-electron occupied vacancy (F+ centers) can behave as described above. However, when F0 centers can overlap with the 4s band, or in the case when a partial compensation would eliminate some electrons from the impurity band, the FM will be favored [3]. Other types/variants of defects were also suspected of playing a role in unusual FM, such as defects introduced at the narrow region of the film-substrate interface, and also defects having two electrons in a triplet ground state or even in excite state formed by a cation vacancy together with a nearby monoelectronic vacancy. Thus, the molecular orbitals in the triplet state may also form an impurity band, replacing the previously discussed BMPs. This band can suffer a spontaneous split (with the condition to be narrow enough) or to interact with the nearby 3d magnetic cations and undergo polarization by exchange with them, events that can occur at quite low concentrations of dopant ions (less or equal with 1%) [3].

Regarding the values of Curie temperatures measured in diluted magnetic oxides and nitrides, some examples were presented by Coey et al. [3]. Thus, in the cases of cation-doped nitrides: GaN-Mn(9%): 940 K, whereas for GaN-Cr: >400 K and for AlN-Cr(7%): >600 K. For titania doped with Co(1–2%): >300 K, with Co(7%): 650–700 K, with V(5%): >400 K, with Fe(2%): >300 K. For tin dioxide doped with Fe(5%): 610 K, with Co(5%): 650 K. For zinc oxide doped with: with: V(15%): > 350 K, Mn(2.2%): >300 K., with: Co(10%): 280–300 K and Ni(0.9%) >300 K. For cuprous oxide co-doped with Co(5%) + Al(0.5%): >300 K. For ITO In1.8Sn0.2O3 doped with Mn(5%): >300 K. All these selected examples show quite high Curie transition temperatures values, many being well above room temperature [3].

Another mechanism for the emergence of FM in diluted magnetic oxide nanoparticles was proposed in [6], and was associated with surface or interior positioned defects in these nanostructures. The authors considered that the FM is manifested in a limited fraction of the nanosized material, which contains zones rich in defects that can also be on the surface, zones being characterized by a narrow ("sharply peaked") local DOS (density of states) in the conditions that the Fermi level (positioned either below or above the mobility edge) will usually not coincide with a local DOS. The authors introduce the concept of a "local charge reservoir" (which contains, for example, dopant cations existing in two different ionized states or is formed by some type of surface charge-transfer complex), which will make possible the increase of Fermi level to a peak in local DOS by electron transfer, named "Stoner splitting" of local DOS. It is highlighted that this spontaneous Stoner FM can occur especially in surface zones that are rich in defects (percolating zones) [6].

Alternative to the bound magnetic polaron BMP model, another mechanism was presented in [7,8] and shortly after described in [9]. Thus, for a certain concentration of holes, the hole "localization length" has a size that greatly surpasses those between acceptors as average. As a result, the holes can now be seen as being delocalized at a length scale that can be compatible with those required for coupling of magnetic ions. As a consequence, the itinerant carriers effectively mediate spin-spin exchange interactions, being possible to be applied proper models such as p-d Zener or Ruderman–Kittel–Kasuya–Yosida (RKKY) on the insulator side of metal-to-insulator transition (MIT), where also important mesoscopic fluctuations in DOS (density of states) can occur [9]. Thus, around the apparent Curie temperature, different paramagnetic and ferromagnetic regions will appear by nanoscale phase separation. The area where the FM order occurs is characterized by ferromagnetic correlation on the long-range between the transitional ions spins that are

randomly positioned. Accordingly, the value of the saturated ferromagnetic moment (and thus the percentage of material enclosing the "ferromagnetic bubbles") increases with the concentration of the net acceptors, extending in all the material on the "metallic side of MIT" [9].

Discussing the origin of ferromagnetic response in DMSs and DMOs, Dietl et al. [9] also invoked as one of the possible causes the phenomenon of spinoidal decomposition (aka spontaneous separation of phases at nanoscale), resulting in regions with a high and low concentration of certain constituents. These separations can result in the formation of nanocrystals embedded in a matrix composed of the predominant component. Yet, because usually this spinoidal decomposition is not accompanied by the formation of macroscopic new crystalline phase, it cannot be observed by X-ray Diffraction (XRD). However, it was possible in some cases to be highlighted by electron microscopy, such as for manganese-doped gallium arsenide, which shows an apparent Curie temperature as high as 360 K [10]. These nanocrystals are stabilized by the surrounded matrix and can be responsible not only for FM, but also for ferromagnetic or antiferromagnetic order [9]. Other examples are chromium-doped zinc selenide [11] or telluride [12] that can be seen not as homogeneous magnetic alloys, but as a collection of non-interacting ferromagnetic particles [9], the latter presenting a maximum apparent Cure temperature of ~320 K for Cr concentrations corresponding to x = 0.2. It is believed that this model can explain the emergence of FM in DMSs and DMOs in the conditions of lack of percolation of magnetic ions in host matrices which do not allow the coupling of nearest neighbors, and also when the concentration of free carriers is not enough to intermediate "efficient long-range interactions" [9].

2. Examples of d^0 Ferromagnetism

2.1. Alkaline-Earth Hexaborides

Borides are a class of compounds which is highly attractive due to their crystal structure and bonding. The boron atoms are held together by strong covalent bonds (also described as "covalent cage structure"), which result in the materials' hardness, having an outcome of high melting temperatures. However, their mechanical features are not the reason why they attracted such attention. Their unique properties come from their electronic conductivity. Hexaborides have a deficiency in charge in their sub-lattice; however, they can gain electrons by "trapping" metal atoms due to the strong boron bonds. Both from an experimental and a theoretical point of view, it has been determined that they can gain two electrons; therefore, generating semiconducting divalent hexaborides and metallic trivalent hexaborides. Among all the properties exhibited by hexaborides, the one that has raised questions is the magnetic behavior of the alkaline-earth hexaborides (MB_6, where M = Ca, Ba, or Br). The reason for this is that, as mentioned above, in order for a material to exhibit magnetism, the main requirement is to have partially-filled d or f bands; however, alkaline-earth hexaborides, such as CaB_6, do not have electros on either d or f bands [13,14]. An example of the crystal structure for CaB_6 is presented in Figure 1.

The first ferromagnetic behavior in alkaline-earth hexaborides was reported by Young et al. in 1999 [15]. In this study, lanthanum-doped calcium hexaborides (CaB_6) exhibited weak ferromagnetic behavior, where some La atoms were replaced by Ca atoms in the structure. It was initially considered that the main reason for this behavior was due to the supplementary electrons introduced by La, generating an excitonic insulator state. Though, later studies reported that weak ferromagnetic behavior was observed even in undoped CaB_6; and was attributed to Ca vacancies generated during synthesis [16]. Undoped CaB_6, SrB_6, and BaB_6 were investigated either as single crystals or as thin films, and they all exhibited weak ferromagnetic behavior at room temperature, which is believed to be a result of intrinsic defects [17–19]. Bao et al. reported the synthesis of alkaline-earth hexaborides and investigated, amongst other features, their magnetic properties. They reported a single-step synthesis route for the fabrication of nanocrystalline hexaborides with tunable particle size. Their results indicated that all samples exhibited weak ferromagnetic behavior at room

temperature. Moreover, their high-resolution transmission electron microscopy analysis suggested that one main factor determining magnetism was their intrinsic defects [20].
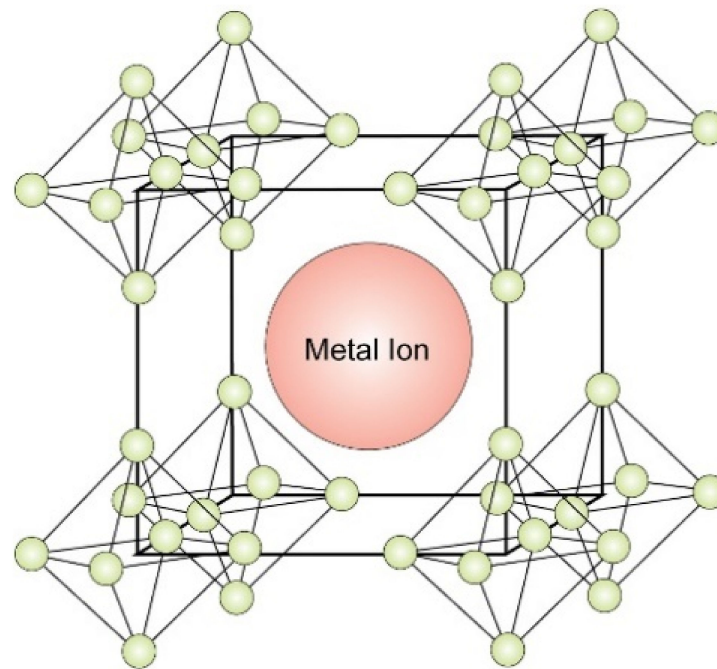
Figure 1. Alkaline-earth hexaboride example of crystal structure (CaB_6) [13].

Recent studies on ternary alkaline earth hexaborides were made to correlate the local structure's deviations with the exhibited ferromagnetism. Using X-ray scattering measurements, Raman spectroscopy, and high-resolution transmission electron microscopy, the local structure of $CaSrB_6$, $CaBaB_6$, and $SrBaB_6$ were investigated. Local symmetry breaking in the B_6 sub-lattice was observed because of displacement disorder, as well as nano-domain generation due to rapid synthesis. The result suggested that the changes in the B_6 sub-lattice may help understand the weak ferromagnetic behavior exhibited by these hexaborides [21].

When discussing CaB_6 specifically, many theoretical points of view have been made in regard to its ferromagnetic behavior. Yet, amongst these, the one standing out is the one that the weak displayed magnetism in CaB_6 is a result of structural defects, such as vacancies in the B_6 lattice. Moreover, there have been studies on the surface of CaB_6 crystals which suggested that ferromagnetism may be determined by magnetic impurities, such as iron. This led to the conclusion that it is needed to investigate whether the transition metal impurities can even carry a magnetic moment. In this regard, Mohanta et al. [14] have conducted ab initio calculations on the magnetic features of transition metal impurities doped in CaB_6. The transition metal impurity atoms calculated were as following: 3d—Sc, Ti, V, Cr, Mn, Fe, Co, Ni; 4d—Y, Zr, Nb, Mo, Tc, Ru, Rh, Pd; and 5d—La, Hf, Ta, W, Re, Os, Ir, Pt. Their results suggested that even though the primary source of magnetism may be B_6 vacancies, an important role is played by the local moments of the transition metal impurity atoms. These atoms could interact by means of conduction electron polarization and generate the weak ferromagnetic behavior exhibited by the material [14].

2.2. Non-Magnetic Oxides

d^0 magnetism in non-magnetic oxides has been a subject of great interest over the past years. However, there have been several controversies over this subject on whether the ferromagnetic behavior is determined by surface defects or impurities [22,23]. Herein, we give examples of some non-magnetic oxides with ferromagnetic behavior and the latest research on the phenomenon. Hafnium, magnesium, cerium, and zinc oxides were

chosen as examples of ferromagnetic behavior in non-magnetic oxides due to their unique properties and extensive use in a wide range of applications. Other oxides, such as titanium dioxide (anatase or rutile phase), tin dioxide, strontium titanate, or zirconia, which were exemplified in Table 1, can also present weak ferromagnetism upon transitional ions doping or even in the undoped state (yet with having certain intrinsic defects).

2.2.1. HfO$_2$

One of the most investigated materials in regard to its unexpected ferromagnetic behavior is hafnium oxide (HfO$_2$). In 2004 it was discovered that HfO$_2$ exhibits ferromagnetic behavior at room temperature in the form of thin films without dopants, which came as a surprise, mainly because Hf^{4+} and O^{2-} are not magnetic ions [24].

Over the last decade, there have been many theories regarding the unexpected ferromagnetic behavior, ranging from impurities to intrinsic defects, such as oxygen vacancies; however, there has not been a consistent conclusion. With the help of theoretical research, it was observed that the generation of magnetism is strongly related to highly concentrated defects that have a magnetic charge configuration. Due to the absence of 3D long-range order, amorphous materials tend to have higher concentrations of intrinsic defects than crystalline materials. Therefore, Qian et al. fabricated amorphous nanostructured HfO$_2$ thin films using a glancing angle deposition technique in order to investigate its ferromagnetic behavior. Their results indicated that the obtained nanostructure exhibited room temperature ferromagnetism without doping which could have been attributed to oxygen vacancies. Moreover, it was observed that morphology strongly affects the intrinsic defects, enhancing the ferromagnetic behavior. Based on SEM and TEM analysis, it was determined that the films had a thickness of around 220 nm with a morphology-based on vertically aligned nano-helices structure. These structures had different screw pitches ranging from 0 to 210 nm; and based on the dimension of the screw pitch, it was observed that the number of spirals is inversely proportional—the smaller the pitch, the higher the number of spirals and the other way around. XPS analysis indicated that there is a difference between the spiral-containing samples and flat film samples. More specifically, the nanosamples with helix structures contained a higher proportion of oxygen deficiency-related peaks and lower proportions for the stoichiometric oxygen peak, correlating to a higher amount of oxygen vacancies than the flat films. Moreover, the analysis results indicated that the nanostructures have a higher bonding configuration for Hf. It was assumed that, due to the fact that the Hf^{4+} ion has a high charge, it polarizes the neighboring oxygen shells; one electron from the oxygen vacancy would occupy the nearby Hf^{4+} ion and yield Hf^{3+} and F$^+$ center resulting in the generation of shallow and deep trap states. The authors proposed that this trapped electron that occupies an orbital overlapping with the unpaired electron of Hf^{3+} is the origin of ferromagnetism in the studied nanostructures [25].

Recent studies on different structures of HfO$_2$ based on first-principle numerical simulations have given some insight into the surface electronic and magnetic properties. The results indicated that there was a clear difference between non-stoichiometric Hf and O-rich surfaces. While both stoichiometric and Hf rich non-stoichiometric surfaces proved not to be magnetic, the O rich non-stoichiometric surfaces exhibited ferromagnetic behavior. Therefore, an O excess surface with asymmetric behavior may be needed to obtain ferromagnetism in simple non-magnetic oxides [26].

2.2.2. MgO

Magnesium oxide (MgO) has a well-known electronic configuration with empty *d*-orbitals and no free electrons. However, regardless of these known parameters, MgO was observed to display room temperature ferromagnetic behavior, mostly attributed to defects and vacancies, either intrinsic or generated by dopants [27–29].

Studies on MgO thin films have shown that the room temperature ferromagnetic behavior is not due to contaminants but rather due to cation vacancies [30]. This was confirmed by later studies on undoped MgO thin films in which the exhibited magnetism

was correlated with the Mg vacancies. Moreover, it was added that there is a link between the crystallinity of the material and the ferromagnetic behavior, in regard to the fact that the magnetism can be enhanced with the decrease in crystallinity [31,32].

A recent study on the matter was conducted on inkjet-printed MgO thin films deposited on Si substrates. After spectroscopic investigations, it was concluded that the magnetization displayed by the MgO thin films was not due to contamination but rather due to Mg vacancies. Moreover, it was observed that vacancy concentrations could be adjusted by the pH value of the ink [33].

Room-temperature ferromagnetism on nanosized powders was also investigated. In a study on MgO powders achieved by thermal decomposition, different phase compositions, morphologies, and magnetic properties were investigated. It was concluded that the room temperature ferromagnetism exhibited as a result of several factors, such as Mg vacancies, the different phase compositions attained by different calcination temperatures, and the degree of crystallinity [34].

2.2.3. CeO_2

Ceria (CeO_2) gained much interest due to its use in environmentally friendly applications for power generation because ceria stores and releases oxygen vacancies [35]. Another known fact about ceria is that stoichiometric CeO_2 is paramagnetic. In order to investigate the magnetic properties of CeO_2, studies were made on different degrees of oxygen-deficient CeO_2. It was observed that the ferromagnetic behavior of CeO_2 can be enhanced by increasing the oxygen vacancy concentration [36].

Early studies on non-magnetic oxide nanoparticles, including CeO_2, showed that all investigated nanoparticles exhibited room-temperature ferromagnetism, while their corresponding bulk form did not. It was believed that the ferromagnetic behavior was due to surface oxygen vacancies that induced exchange interactions between unpaired electron spins and it was suggested that room-temperature ferromagnetism could be exhibited in all metal oxides in the form of nanoparticles [37,38]. Other studies on the matter determined that a ferromagnetic behavior in CeO_2 nanostructures could be present only in structures that have less than 20 nm. Moreover, the study excluded the possibility of ferromagnetic behavior induced by impurities or oxygen vacancies [39]. Fernandes et al. investigated the ferromagnetic behavior of CeO_2 films both experimentally and theoretically. They concluded that the exhibited magnetism is due to structural defects which are attributed to cerium and oxygen vacancies [40].

Recent studies suggest that the structures of the vacancies that induce magnetic defects strongly depend on the crystallographic surface, as well as the temperature regime used on CeO_2 nanoparticles [41]. A combination between defects, disorder, and non-stoichiometry in nanostructured CeO_2 might be the main reason for the unexpected ferromagnetic behavior [42].

CeO_2 transparent thin films in regard to their magnetic behavior were investigated at high temperatures. It was observed that the changes in the electronic structure cannot be the only reason for the unexpected exhibited ferromagnetism. The results indicated that the magnetic moments are strictly linked to oxygen vacancies [43].

2.2.4. ZnO

Another interesting oxide is ZnO, and its attractiveness from an experimental point of view is the fact that it is low-cost and is widely used in a various range of applications. ZnO gained considerable attention due to its possible use in spintronic applications [44]. As early as the year 2000, studies had been published on the generation of ferromagnetism in non-magnetic oxides by doping them with magnetic ions [8]. There were various studies on the origin of ferromagnetism in ZnO, both theoretically and experimentally. However, even so, the reason for ferromagnetism in ZnO is still debated. Some have suggested that the carrier-induced ferromagnetic behavior of ZnO can be controlled by modifying the carrier's density (electron or hole concentrations depending on the amount

of dopant—cations or/and anions—introduced) [45,46]; other investigations on the room temperature ferromagnetic behavior of un-doped ZnO single crystal have shown that it was induced due to oxygen vacancies generated by thermal annealing in Ar flow [47]. Moreover, the ferromagnetic behavior can be induced in ZnO (or other non-magnetic oxides) by doping [48].

An idea that caught the attention of several researchers is that the exhibited ferromagnetism is related to grain boundaries. In 2009, an explanation was proposed in the hope of elucidating contradictory findings. They observed that bulk doped or un-doped ZnO does not exhibit ferromagnetic behavior. Further investigations showed that only polycrystalline ZnO with a high specific area of the grain boundaries showed ferromagnetism, irrelative to doping [49]. Studies on un-doped ZnO nanoparticles attributed the exhibited room temperature ferromagnetic behavior to lattice defects. Moreover, doping the above-mentioned nanoparticles with first group elements led to an enhancement in the ferromagnetic behavior [50].

Room temperature ferromagnetic behavior was observed in pure ZnO nanoparticles. By varying experimental parameters, it was concluded that an important part in the generation of ferromagnetism in ZnO nanoparticles is played by oxygen vacancies [51]. Following this idea, the correlation between particle size and oxygen vacancies was investigated. The synthesized nanoparticles had a particle size of 6, 7, and 11 nm. It was observed that decreasing the particle size leads to an increase in oxygen vacancies, leading to a long-range ferromagnetic ordering in these nanoparticles. It was concluded that a crucial role in room temperature ferromagnetic behavior exhibited in un-doped ZnO nanoparticles is attributed to oxygen vacancies which can be controlled by particle size [52].

2.3. Carbon Nanostructures

Magnetism in carbon-based materials has gained a great deal of attention during the past years, both theoretically and from an application point of view. Theoretically, it is an *sp*-electron-induced magnetism against the basic idea that only materials with *d* or *f* electrons could exhibit room-temperature ferromagnetism. From an application-based standpoint, magnetic carbon is an encouraging material for spintronics, electronics, and biomedicine. Magnetic susceptibility values for carbon polymorphs show that it is usually diamagnetic. However, it was observed that organic materials which do exhibit ferromagnetism do so at very low temperatures; furthermore, study results of intrinsic magnetism of materials based on pure carbon have been controversial, mainly due to possible magnetic impurities [53,54].

2.3.1. Fullerenes

Fullerenes were discovered in 1985 by Kroto et al. [55]. The most stable fullerene is C_{60}, and even though in its un-polymerized form it is considered to be diamagnetic, there have been reports of fullerene-based structures that exhibited ferromagnetism [56]. The first report of ferromagnetic behavior in the polymer-C_{60} was observed in 1994 by Ata el., when C_{60} was ultrasonically dispersed in a dimethylformamide solution of polyvinylidene fluoride [57]. Since then, there have been numerous reports on fullerene-based structures with ferromagnetic behavior.

It has been observed that the magnetic behavior exhibited in polymerized fullerenes is strongly related to certain preparation conditions, such as temperature, pressure and time [58]. For example, the appearance of ferromagnetic behavior was noticed in conditions where the fullerene structure is almost destroyed. This effect was believed to be correlated with intra-molecular defects [59]. The effect of pressure and temperature was also confirmed in a study on rhombohedral C_{60} polymer by generating different degrees of ferromagnetic behavior [60]. Another mechanism of induced ferromagnetism was observed in C_{60} crystal when irradiated by light in oxygen [61]. An interesting example of exhibited ferromagnetism is a system composed of Pd/C_{60} bilayers. Intriguingly, neither

C_{60} nor Pd films are ferromagnetic; however, experimental and theoretical studies showed ferromagnetic behavior in stacked bilayers of Pd/C_{60} [62].

2.3.2. Graphene

Apart from the already known unique properties of graphene, several studies reported that ferromagnetic ordering could be found within the structural defects [63–65]. In a first-principle calculation study on nano-flakes graphene, it was shown that the zig-zag-edged structure of these nano-flakes could contribute to the exhibited ferromagnetic behavior [66]. Room temperature ferromagnetism was noticed in bulk graphene materials obtained from soluble functionalized graphene sheets, which was attributed to the structural defects of graphene [53]. Graphene-based materials with incorporated magnetism could be promising candidates for spintronic applications. Enhanced ferromagnetism was obtained by modifying edge state morphology in graphene nanoribbons [67].

Twisted bilayer graphene has been recently intensely researched in regard to its potential ferromagnetic behavior. This system is basically composed of two sheets of graphene, which are superimposed with a slight twist angle between them. By misaligning the two graphene sheets relative to each other, a moiré pattern is formed. Recently, it was demonstrated that three-quarters filling of the conduction band leads to the induction of a ferromagnetic state [68].

Stabilizing the room temperature ferromagnetic ordering in materials based on graphene remains a significant challenge due to the wide area of applications in which they could be used, such as spintronics, electronics, biomedicine, and separation technologies [69–73].

2.3.3. Graphite

The ferromagnetic behavior of graphitic materials has been strongly linked to lattice defects. For example, there have been studies on the irradiation-induced magnetism for graphite. Based on a comparison between the magnetic properties of the defects that are likely to be generated due to irradiation vacancies or H vacancy complexes, the results indicated that even though they are both magnetic, the adsorption of H greatly increases the magnetic moment [74]. Pure bulk graphite was investigated and showed ferromagnetic behavior attributed to the material's topographic defects [75].

Ion-implanted graphite is of extreme interest due to generating lattice defects, such as vacancies, in a controlled manner. Due to the unpaired electrons resulted from the ion beam, the induced defects could present magnetic moment. C^+ ion-implanted graphite was investigated in several studies. The results indicated that the exhibited ferromagnetism could mostly be attributed to the induced vacancy defects by implantation [76,77]. Recent studies showed the generation of "comet-like" defects by swift heavy ions in highly ordered pyrolytic graphite. The analysis suggested that these types of defects have considerably higher magnetic signals in comparison to intrinsic surface defects [78].

Esquinazi et al. discuss the detection of FM in various highly crystalline graphite materials and the three main possible explanations for this behavior. The highest magnetization found was ~2.5 memu/g at room temperature with a high Curie transition Tc~900 K [79].

The magnetic impurities, such as as metallic iron or magnetite clusters, cannot be responsible for the observed magnetization due to higher Ms value measured (in some samples) towards those which would be provided by a magnetic impurity, doubled by the fact that the magnetic impurities should have a superparamagnetic and not a ferromagnetic behavior, as observed with HOPG samples. Thus, graphite samples magnetization remains practically temperature independent up to 800 K, contrasting with Fe superparamagnetic behavior, which sharply decreased with increasing temperature [79].

Topological defects, especially grain boundaries and edge states (the zig-zag edges), can induce an increase in DOS. If there is a high enough density of edge stated, it was considered that it can induce a ferrimagnetic spin polarization. Moreover, from theoretic data, it was suggested that a strong topological disorder will inhibit antiferromagnetic order while the ferromagnetic order will be enhanced [79].

Itinerant ferromagnetism can play a role in graphite FM, since this material has a low carrier density and the inter-electronic interaction is large in such "dilute 2D electron gas systems". Indirect evidence of this graphite electrons interactions was obtained from magnetoresistance analyses which revealed a "field-induced metal-insulator-like transition" [79]. Moreover, the powerful Coulomb interaction can lead to opening a gap in graphite Dirac fermions which is doubled by the detection of a weak magnetic moment induced by band anisotropy. Additionally, CESR (conduction electron spin resonance) measurements on HOPG and other highly crystalline graphite, such as Kish graphite, detected the presence of a ferromagnetic-like inner field. The authors underlined that the spin polarization and excitonic gap were induced by the Coulomb interaction even for the case when the magnetic field is absent. However, if a magnetic field is perpendicularly applied on the graphite sheets, even if the Coulomb interactions were weak, it can induce the gap formation [79].

The role of the defects in the graphite FM was also studied in [77]. Carbon ion implantation was used in the HOPG technique, which generated insulated and clustered vacancies. The room temperature (RT) FM in the irradiated graphite samples was directly correlated with the presence of generated vacancy defects. From the simulations, the authors detected, as a source of magnetic defects in graphite, some particular configurations such a V1 (single vacancy with three dangling bonds in a 12 C atoms ring), V6 (18 carbon atoms ring with six dangling bonds), and some V4 structures (also having 12 C atoms ring yet with two dangling bonds). The authors also inferred the possibility of tunning the magnetization in different carbon forms via controlling the density of the induced defects [77].

2.3.4. Carbon Nanotubes

Carbon nanotubes have been widely used in nanotechnologies due to their unique properties [72,80]. Magnetic carbon nanotubes could open a whole new range of applications. Studies on the possible magnetization of carbon nanotubes when in contact with a magnetic material were conducted. Results indicated that spin-polarized charge transfer occurs when a carbon nanotube is in contact with a ferromagnetic material, leading to the magnetization of the carbon nanotube [81]. Room temperature ferromagnetism was also observed in hydrogenated carbon nanotubes. The mechanism proposed here was based on the introduction of hydrogen in a disordered nanotube structure, thus facilitating the hydrogen uptake and inducing a ferromagnetic moment. Moreover, it was observed that the ferromagnetic behavior was dependent on temperature and nanotube wall thickness [82].

A recent study proposed a nitrogen plasma treatment protocol for the treatment of carbon nanotubes with the purpose of ferromagnetism enhancement. The results suggested that the main reason for the ferromagnetic behavior is granted to the bonding configuration between pyridine and amine N [83]. Room temperature ferromagnetism was also observed in single-walled carbon nanotubes. Recent experiments on this subject excluded the possibility of impurity-induced magnetism but rather attributed it to carbon vacancies [84].

Table 1. Comparison between different material magnetization and their potential mechanism.

System	Ref	Saturation Magnetization (M_S)	Observations	Species Responsible for Ferromagnetic Behavior
Non-magnetic oxides				
ZnO nanowire (NW) arrays	[85]	2.3 emu/cm^3 (0.41 emu/g) at T = 300 K	The magnetic field applied parallel to the growth direction of elongated nanostructures.	- O 2p orbitals; - considerable local spin moment in the nearest-neighboring O atoms regarding the defect center generated by Zn vacancies
ZnO nanocactuses on ZnO NW arrays		3.1 emu/cm^3 (0.55 emu/g) at T = 300 K		
Tryoctylphosphine capped-ZnO nanoparticles (NPs)	[86]	3 memu/g at T = 5 K	The sp conduction band is where the magnetic polarization of the Zn atoms is attained.	- the hybridized band formed by Zn and the bonding atom of the molecule
Dodecylaminne capped-ZnO NPs		2.5 memu/g at T = 5 K		
Dodecanethiol capped-ZnO NPs		2.6 memu/g at T = 5 K		
ZrO$_2$ Mn-doped thin films	[87]	20% Mn (cubic phase) 0.83–0.96 emu/cm^3 (0.15–0.17 emu/g) at T = 5 K 10% Mn (monoclinic phase) 0.36 emu/cm^3 (0.06 emu/g) at T= 5 K	At T = 5 K -> H_c coercive fields = 95 and 205 Oe.	- structural defects - the films with cubic phases exhibit a higher dislocation density which has been associated with the increase in magnetization
ZnO single crystals	[88]	6.3×10^{-5} emu/g T = 300 K (untreated sample) 1.6×10^{-4} emu/g T= 300 K (treated)	Curie temperature > 300 K.	- oxygen vacancy generated as a result of thermal annealing in argon flow

Table 1. *Cont.*

System	Ref	Saturation Magnetization (M_S)	Observations	Species Responsible for Ferromagnetic Behavior
Li, Na, and K-doped ZnO NPs	[50]	ZnO: 0.129×10^{-3} emu/g Zn$_{0.95}$Na$_{0.05}$O: 0.094×10^{-3} emu/g Zn$_{0.95}$K$_{0.05}$O: 0.219×10^{-3} emu/g Zn$_{0.95}$Li$_{0.05}$O: very weak ferromagnetic + diamagnetic at T = 300 K	Ion doping enhances FM behavior through exchange interactions. Decreased FM behavior for Li-doped ZnO at higher field.	- room temperature FM observed due to V_O^+ trapped unpaired electrons
K-doped ZnO films	[89]	0%K: 4.4 emu/cm^3 (0.79 emu/g) 4%K: 6.1 emu/cm^3 (1.09 emu/g) 6%K: 7.3 emu/cm^3 (1.3 emu/g) 8%K: 10.7 emu/cm^3 (1.91 emu/g) 11%K: 3.5 emu/cm^3 (0.63 emu/g) at T = 300 K	Maximum M_S value at 8% K content.	- localized holes due to Zn vacancy and K$_{Zn}$ defects
ZnO NPs	[90]	250 °C annealed: 0.004 emu/g 500 °C annealed: 0.0042 emu/g 750 °C annealed: 0.0024 emu/g 1000 °C annealed: 0.0018 emu/g at T = 300 K	By increasing the annealing temperature, the M_S decreases.	- oxigen vacancies - intrinsic ferromagnetic ordering in ZnO NPs could be due to surface defects.

Table 1. *Cont.*

System	Ref	Saturation Magnetization (M_S)	Observations	Species Responsible for Ferromagnetic Behavior
ZnO thin film	[91]	150 °C annealed: 0.08 emu/g 600 °C annealed: 0.42 emu/g at T = 300 K	- induced defects by thermal annealing in argon flow	- singly occupied oxygen vacancy
ZnO NPs	[92]	Raw NPs: diamagnetic after 50 h milling: 0.031 emu/g after 100 h milling: 0.047 emu/g after 200 h milling: 0.086 emu/g at T = 300 K	- induced defects by mechanical milling in diamagnetic ZnO powders - increased density of defects leads to increased FM order - H_c = 20–90 Oe	- oxygen and zinc vacancies associated intrinsic defects
ZnO high pure (99.999%) sinthered bulk ceramics	[93]	500 °C sintered: 0.0183 emu/g 850 °C sintered: 0.0190 emu/g 1300 °C sintered: 0.00188 emu/g at T = 300 K	H_c = 1300 Oe H_c = 12 Oe H_c = 34.4 Oe	- cation/anion (Zn/O) defects, as well as interstitials generated by sample processing
ZnO Gd or Gd + Mn-doped NPs	[94]	Undoped NPs: Diamagnetic Gd-doped NPs: 0.15 memu/g Gd + Mn-doped NPs: 0.11 memu/g	The magnetization for Gd-doped NPs did not saturate at high magnetic fields. Mn ions suppressed FM behavior.	- room temperature FM (Gd-doped ZnO NP) possibly due to oxygen vacancy - s-f coupling between ZnO and Gd ions
ZnO Cu-doped short facetted microrods or microtubes	[95]	Pure ZnO: Diamagnetic ZnO-Cu 0 T: 0.008 emu/g ZnO-Cu 4 T 0.012 emu/g at T = 298 K	Improved M_S by applying a pulsed magnetic field at the time of synthesis.	- magnetic polarons generated by the oxygen vacancies and Cu^{2+} ions

Table 1. *Cont.*

System	Ref	Saturation Magnetization (M_S)	Observations	Species Responsible for Ferromagnetic Behavior
TiO_2 films on Si substrates	[96]	P_{O2} = 50 mtorr: diamagnetic P_{O2} = 0.2 mtorr Very weak ferromagnetic+ Diamagnetic ~0.02 emu/cm^3 (~0.005 emu/g) P_{O2} = 0.02 mtorr ~0.3 emu/cm^3 (~0.075 emu/g) At T = 298 K	A clear relationship between the magnetic moment and the concentration of oxygen vacancy	- oxygen vacancies
TiO_2 films	[97]	Anatase film: 2 emu/cm^3 (~0.52 emu/g) Rutile film: 6 emu/cm^3 (~1.42 emu/g)	Vacuum annealing could produce a finite supply of oxygen vacancies.	- oxygen vacancies for rutile films
TiO_2 anatase H_2 annealed 12 h at 600 °C	[98]	Pristine TiO2 very weak paramagnetism TiO2:H 0.066 emu/g H_c = 171 Oe T_C ~ 450 K	Local 3*d* moments generated by hydrogenation.	- Ti3+ and oxygen defect complexes - oxygen vacancy - Ti 3d-O 2p hybridization

Table 1. *Cont.*

System	Ref	Saturation Magnetization (M_S)	Observations	Species Responsible for Ferromagnetic Behavior
TiO_2 rutile single crystals doped with transitional metal ions (TM = Cr, Mn, Fe, Co, Ni, Cu)	[99]	TiO_2 undoped 0.013 emu/mol (0.16 memu/g) TiO_2-Cr 0.029 emu/mol (0.36 memu/g) TiO_2- Mn 0.044 emu/mol (0.55 memu/g) TiO_2- Fe 0.110 emu/mol (1.36 memu/g) TiO_2- Co 0.017 emu/mol (0.21 memu/g) TiO_2- Ni 0.069 emu/mol (0.86 memu/g) TiO_2- Cu 0.012 emu/mol (0.15 memu/g)	The results suggest a precise superposition of a feromagnetic and paramagnetic behavior.	- the separation of metallic Fe, Co, and Ni phases - unpaired d electrons from transitional metal ions
TiO_2 Co-doped polycrystalline pellets	[100]	TiO_2 diamagnetic $Ti_{0.95}Co_{0.05}O_2$ 0.07 emu/g $Ti_{0.95}Co_{0.05}O_2$:H 2.35 emu/g * $Ti_{0.95}Co_{0.05}O_2$:Htd 0.08 emu/g At T = 300 K *Also at T = 50 K	Co-doping generated weak ferromagnetic ordering; however, when annealed in H atmosphere, there is a significant increase in the magnetization. Furthermore, reheating in air reverses the effect to the original.	- oxygen vacancy generated by Co^{2+} substitution and enhancd by hydrogenation

Table 1. *Cont.*

System	Ref	Saturation Magnetization (M_S)	Observations	Species Responsible for Ferromagnetic Behavior
SrTiO$_3$ single crystal	[101]	H$^+$ ions irradiated $\sim 1.3 \times 10^{-3}$ emu/cm^2 N$^+$ ions irradiated ~ 4.2–6.2×10^{-4} emu/cm^2 At T = 300 K	FM reduced when secondary oxygen-deficient phases increased	- oxygen vacancies
SnO$_2$ high purity powders	[102]	0 h milled 0.6 memu/g 4 milled 1.9 memu/g 12 h milled 5.5 memu/g 20 h milled * 10.5 memu/g	*20 h milled sample was then heated In air 4 h at diff temp. 0 °C 8.7 memu/g 200 °C 3.8 memu/g 400 °C 1.9 memu/g 600 °C 0.8 memu/g	- high defect density—singly charged oxygen vacancies
SnO$_2$ NPs	[103]	Raw powder 0.019 emu/g Annealed at 500 °C 0.015 emu/g Annealed at 700 °C 0.012 emu/g Annealed at 900 °C 0.010 emu/g Annealed at 1100 °C 0.006 emu/g Annealed at 1300 °C 0.001 emu/g Measured at T = 300 K Coercivities ~181–206 Oe	Raw powder 0.75 emu/g Annealed at 500 °C 0.54 emu/g Annealed at 700 °C 0.23 emu/g Annealed at 900 °C 0.019 emu/g Annealed at 1100 °C 0.13 emu/g Annealed at 1300 °C 0.05 emu/g Measured at T = 5 K Coercivities ~178–187 Oe	- oxygen vacancies (T = 5 K)

Table 1. *Cont.*

System	Ref	Saturation Magnetization (M_S)	Observations	Species Responsible for Ferromagnetic Behavior	
SnO_2 films on $LaAlO_3$ substrates	[104]	10 nm film ~27 emu/cm^3 (~3.94 emu/g) 220 nm raw film ~12 emu//cm^3 (~1.75 emu/g) 220 nm 700 °C O_2- post-annealed film for 10 h ~diamagnetic At T = 300 K	the magnetic field is applied parallel to the film's plane	-	oxygen vacancies near the surface
Sr_3SnO film	[105]	~7 emu/cm^3 (1.48 emu/g) At T= 300 K	Hc ~75 Oe	- -	intrinsic defects cation vacancies
CeO_{2-x} films	[40]	For x = 0.03 ~1.34 emu/g For x = 0.1 ~1.02 emu/g At T = 300 K	Both Ce^{4+} and Ce^{3+} ions are present	-	oxygen and cerium vacancies
HfO_2 films	[106]	128 emu/cm^3 (~13.223 emu/g)	Vacuum and air annealing clearly affected FM	- -	porous structure of the film oxygen vacancies
MgO films	[32]	~2.69 emu/cm^3 (~0.751 emu/g) After annealing treatment: 1.18 emu/cm^3 (~0.329 emu/g)	Reduction of Ms after annealing related to a reduction of Mg vacancies.	-	Mg cation vacancies

Table 1. *Cont.*

System	Ref	Saturation Magnetization (M$_S$)	Observations	Species Responsible for Ferromagnetic Behavior
Alkaline-earth hexaborides				
CaB$_6$ films	[107]	Thickness: 0.5 μm 11.36 emu/cm^3 (~4.63 emu/g) Thickness: 1.6 μm 1.136 emu/cm^3 (~0.463 emu/g) Thickness: 2.3 μm 0.25 emu/cm^3 (~0.102 emu/g)	Increasing the thickness resulted in Ms decrease. Results ruled out iron contamination.	- defects determined by lattice distortion and grain boundary
CaB$_6$ crystal	[108]	0.12 emu/cm^3 (~0.0489 emu/g)	FM mostly on/near the surface of the sample	- surface contamination.
BaB$_6$ thin film	[19]	10.7 emu/cm^3 (~2.454 emu/g) at T = 450–550 °C	Results ruled out contamination. No variations due to film thickness.	- film defects
Carbon nanostructures				
Highly-oriented graphite samples	[79]	AC1-HOPG 1.39 memu/g AC2-HOPG 0.33 ± 0.04 memu/g UC2-HOPG 0.83 ± 0.03 memu/g UC3-HOPG 1.1 ± 0.2 memu/g HOPG-2 0.93 ± 0.1 memu/g HOPG-3 2.5 memu/g Kish graphite 0.6 ± 0.2 memu/g At T = 300 K	Different possibilities for the FM-like behavior in the samples.	- magnetic impurities - topological defects - itinerant ferromagnetism

Table 1. *Cont.*

System	Ref	Saturation Magnetization (M_S)	Observations	Species Responsible for Ferromagnetic Behavior
C_{60}	[60]	0.045 emu/g T ~ 800 K	Pressure used 9 GPa. Results indicate a reduction in the ferromagnetic behavior after 800 K.	- carbon radical formation
Graphene	[53]	Annealing temp 400 °C At 300 K—0.004 emu/g At 2 K—0.25 emu/g Annealing temp 600 °C At 300 K—0.020 emu/g At 2 K—0.90 emu/g	Graphene prepared at 800 °C showed no clear sign of FM.	- defects generated through annealing
Graphene nanoribbons	[67]	1.1 emu/g	Optimization of density zig-zag edge defects.	- defect density
Highly oriented pyrolytic graphite—$^{12}C^+$ ion implantation	[76]	14.4 emu/g	Increase of implantation steps correlated with the increase in vacancy density.	- vacancy density
Carbon nanotubes	[83]	0.5227 emu/g	N_2 plasma treatment.	- bonding configuration of N pyridine and amine

3. Drawbacks of Unexpected Ferromagnetism

Even though there are many decades of studies on the presence of weak ferromagnetism in systems such as diluted magnetic semiconductors and oxides, and also in many other exotic systems, there is still much controversy about the origin of this phenomenon, despite the different theoretical models. For example, donor impurity band exchange, implying bound magnetic polarons; or charge-transfer ferromagnetism for doped oxide nanoparticles [8] developed and employed to explain their behavior. The study on this class of materials is also hampered by the high dependence of the magnetic properties on the synthesis method, their morphology (bulk, thin films, nanoparticles, etc.), and the presence of surface defects [109]. Moreover, there is also the problem of reproducibility and contamination of samples with unwanted magnetic impurities.

For example, single-phase iron-doped zinc oxide ceramics obtained by solid-state reaction, having $Zn_{1-x}Fe_xO$ ($0 \leq x \leq 0.07$ mol) composition, showed a weak superparamagnetic behavior without a clear saturation of hysteresis magnetization curve even at magnetic fields as high as 18 kOe, while the corresponding magnetization values increased from 0.02 emu/g at 1% Fe up to 0.18 emu/g at 7% Fe [110]. Additionally, ZnO-Fe-doped nanoparticles synthesized by sol–gel auto-combustion method [111], having $x = 0.02, 0.04, 0.06$ and 0.08, presented a similar tendency with magnetization values approaching 0.85 emu/g at 2000 G for the highest dopant concentration. Wheres pure ZnO presented a much lower magnetization (4×10^{-5} emu/g) at the same external field value. However, studies performed on ZnO single crystals implanted with Fe ions and analyzed by Mossbauer spectroscopy and X-ray magnetic circular dichroism (XMCD) revealed that, at a very low doping regime (10^{-5} at.%), only isolated paramagnetic trivalent iron ions had "a spin-lattice type of relaxation", whereas at higher Fe^{3+} doping regimes (0.02–0.2 at%) the relaxation between nearby iron ions becomes spin-spin type, and at even higher concentrations, up to 2.2 at.%, the researchers did not find any signature of magnetic ordering [112]. Thus, they concluded that, oppositely to other observations of dilute magnetism in zinc oxide systems doped with 3d ions, there was "no evidence of any long-range magnetic ordering between isolated Fe atoms incorporated in the ZnO lattice" [112]. Thus, it seems that, without an efficient mechanism for mediating long-range interactions, there is no magnetic ordering at room temperature in this wide band gap and "truly diluted" oxides/semiconductors, the authors implying that the cause for this could be the conditions of the absence of precipitation or 3d–aggregates or surface contaminants [112].

In their article revising the topic of d0 ferromagnetism in undoped zinc oxide nanostructures [113], the authors summarized the possible origin of erroneous magnetic signals foreign to measured samples, which can be applied to other diluted magnetic materials. Thus, small influences that are not very important for materials with strong magnetization start to compete with the true magnetic signals when one deals with very weakly magnetic materials, such as those from the undoped zinc oxide class whose magnetization is around or even smaller than $\sim 10^{-4}$ emu [114]. Two different categories of sources of possible errors when these samples were manipulated for magnetic measurements using SQUID (superconducting quantum interference devices) or VSM (vibrating sample magnetometers) were identified:

- Material contaminations in a homogeneous manner which seems to be proportional to their weight and can be identified by careful chemical analysis; and
- Specific contaminations during the procedure of measurement, which include the sample fixation in a certain geometry inside apparatus and that can produce a false signal, which do not depend on the sample mass and can be due to stainless-steel tools such as tweezers or fine blades, polyimide Kapton tape, plastic tubes (straws), gelatin capsules, cotton, silver conductive paint, and inks iron/iron oxide-contaminated or even anisotropy artifacts [114]. For example, the sticky Kapton tape, which is usually employed to attach the samples on their holders, can be simply contaminated by magnetic air dust microscopic particles and can induce ferromagnetic or paramagnetic signals between 10^{-4} and 10^{-5} emu [113].

Moreover, due to the fact that the magnetic measurements in SQUID or VSM are based on the principle of magnetic induction in a nearby coil, which occurs when a variable magnetic flux across the coil is used, this flux will be influenced by the sample magnetic moment and also by the sample orientation and distance towards the center of coil, thus the resulted magnetic signal in the case in inhomogeneous contamination will depend by the sample position [113].

Moreover, the sources of ferromagnetism that are foreign to the sample associated with integral magnetometry measurements, especially by SQUID technique, were carefully revised in a more recent paper by L.M.C. Pereira et al. [115]. He also found two categories of possible errors: The first being related to the experimental setup that results in misidentification of the magnetic state of the sample and the second being considered as accidental magnetic contaminations, as classified in [113], which cannot necessarily be only those deposed on sample surface but also can be incorporated in the sample [115]. The SQUID device itself can be capable of "emulating ferromagnetism where it does not exist", due to the generation in some cases of a residual ferromagnetic-like hysteresis curve, due to differences in the ideal behavior of power supply and the magnetic superconducting coil [113]. They also classified the sources of contamination as being from cleaning and handling, sample mounting (where the constraints of the free-standing method were highlighted), sample substrate, and high-temperature processing and/or annealing of the sample (problem of contamination by evaporation/condensation of heated metallic parts), finishing with "accidental contamination even in metal-free conditions" (by solvents/ ultra-sonication) [115]. Additionally, the author of [115] discussed the instrumental artifacts in three paragraphs:

- False (spurious) ferromagnetism originating from the magnetometer magnetic field non-uniformity, resulting in errors that become important for the case of nanomaterials with a magnetic signal much lower than those of the diamagnetic signal of their substrate;
- Features associated with non-intrinsic ferromagnetism (such as those derived from the asymmetry of ferromagnetic volume versus the center of the moment in the case of the uniformly magnetized diamagnetic sample);
- Intrinsic-like features associated with non-intrinsic ferromagnetism (anisotropy artifacts linked to axial or radial effects).

The difficulty of the study of the intrinsic FM in dilute magnetic nanomaterials is considered in [115] to be related to their complicated phase diagrams, not only from the structure point of view but also from the magnetic behavior. From the first, these materials can be situated from truly diluted systems up to more or less segregated systems. From the second, from paramagnetic having non-interacting local moments to systems having various intensities and ranges of magnetic interactions, accompanied by different types of magnetic order [115].

4. Applications and Future Trends

One of the potential applications for diluted magnetic oxides (and possibly other materials having "diluted" magnetic properties) is the obtaining of performant materials that simultaneously possess electric and magnetic properties, eventually combined with transparency for use in electronics. The other major target for these materials is their promising application in spintronics due to their expected controlled spin-polarization carriers injection [116]. The spintronics (abbreviation for spin-transport electronics) domain is based on the study of the electron spin and their associated magnetic moment for the applications in efficient solid-state devices, such as those for data storage and information transfer, as briefly reviewed in [117]. In the same review [117], the authors believe that an "ultimate goal for spintronics" in the longer term is to replace the CMOS (complementary metal-oxide-semiconductor) transistor with an equivalent device using extremely low power. From the spintronic point of view, their electrical charge and the spin of electrons are controlled to operate the information circuits [116]. Consequently, this kind of manipulation

of spins (from electrons or holes) in semiconductors has immense potential from high-speed information processing, accompanied by their storage in non-volatile memory using low power, and can open a path for quantum computing [116,118]. Other spintronic devices based on magnetic semiconductors are spin-field emission transistors (spin-FETs) and spin logic gates [119]. The authors from [116] enumerate some of the technical problems that need to be resolved in order for the spintronics to be industrially feasible: "efficient injection, transport, control and manipulation, and detection of spin polarization and spin-polarized currents".

Pan et al. [120] carefully revised the vast domain of zinc oxide films doped with transitional ions (such as monodopants Co, Mn, Sc, Ti, V, Cr, Fe, Ni, Cu, and also with FeCu, CoCu, CoFe, CoAl, MnCo, MnSn, MnAl, MnN, MnP, MnP, MnCu, CuGa, CoLi, CoN, CuN, as pairs of co-dopants) for possible applications in spintronics, highlighting that there still remains a lot of questions about its origin as well as the use for spintronics [120]. In turn, the authors concluded that the origin of room temperature ferromagnetism in these systems was unambiguously proved to be the structural defects, pointing out that the carriers responsible for carrier-mediated exchange were only "natural byproducts" of the defect creation in these zinc oxide-based materials [120]. Moreover, they claim that spintronic devices of second-generation, containing these ZnO special films with not only ferromagnetic but also with piezolelecrric, ferrelectric, and optical properties, can be fabricated devices that can induce and manipulate spin-polarized electrons (or holes) in a semiconductor [120].

Magnetic tunnel junctions (MTJs) are devices whereby the tunneling of electrons through the dielectric layer is controlled by their spin via the electrodes made from ferromagnetic materials, which can have parallel or antiparallel magnetizations [121]. For example, in [122] a functional MTJ device is described as having one electrode made from a co-doped rutile TiO_2 FM semiconductor, the other being metallic ($Fe_{0.1}Co_{0.9}$) separated by an AlOx dielectric barrier. Thus, the $Ti_{1-x}Co_xO_{2-\delta}$ film was demonstrated to be able to act as a spin injection electrode in this device, having a TMR ratio of ~11% at 15 K [122]. Unfortunately, in this case, the TMR diminished as the temperature increased and disappeared at 180 K due to the low quality of amorphous alumina barrier, which induces inelastic tunneling conduction at higher temperatures [122]. Another example presented in [122] is the device based on an all-oxidic tri-layer FM-insulator-FM $Zn_{0.94}Co_{0.06}O$ (25 nm)/MgO (4 nm)/$Zn_{0.94}Co_{0.06}O$ (50 nm), which showed a TMR ratio of 46.8% at 2T magnetic field but at the very low temperature of only 2 K. The value of the $V_{1/2}$—the bias voltage where the TMR ratio is half of the zero-bias value observed—was very high (10 V), which encouraged the authors to see a potential application in MRAM (magnetoresistive random access memory) devices or in reading heads for hard disks—applications requiring a high voltage bias [122]. A similar all-oxidic device was presented in [123], where all three layers contain epitaxially grown zinc oxide: $Zn_{0.94}Co_{0.06}O$ (50 nm)/ZnO (4 nm)/$Zn_{0.94}Co_{0.06}O$ (25 nm). The researchers found a TMR positive ratio of 20.8% at 4 K that can exist (while much diminished) even at room temperature, whereby the TMR ratio was 0.35% at 2T due to a better crystallinity of both barrier and barrier–electrode interfaces, accompanied by a reduced bias-dependence TMR, which is promising for the Gb-scale MRAM [123].

For reliable spintronic devices, a major problem encountered was the efficient "transfer of the spin-polarized carriers from a magnetic contact into a nanomagnetic semiconductor", and one method to achieve this goal was to use—in the ambient conditions—a polarized laser light (optical pumping) [116]. However, for the electronic device integration, an electrical spin injection approach will be required [116]. Unfortunately, it is very difficult to obtain a good spin injection efficiency in the case of the interface between a DMO and semiconductor (the source and the channel), coupled with an efficient spin detection at the chain–drain interface, all these being required for performant spin-field emission transistors [116].

Another direction of applications of DMS and DMO is the potential to influence the magnetization not by an external magnetic field but by using an electrical field, which can

be of great importance for the field of spintronics for device applications. As was demonstrated for the first time in [124] for the case of the Mn-doped indium arsenide thin-film magnetic semiconductor using an insulating-gate field-effect transistor. In addition, in an Mn-doped gallium arsenide [125], where it was concluded that the control of carriers (holes) concentration and of magnetic anisotropy was achieved via applied electric field on a metal-insulator-semiconductor device, which allowed for the manipulation of the magnetization direction, opening the path for non-volatile devices that do not need the intervention "of a magnetic field, spin current, or mechanical stress". A drawback of these materials is their Curie temperatures, which are usually low (below 190 K) [116]. However, another report [126] presented an epitaxial $PbZr_{0.2}Ti_{0.8}O_3/Co:TiO_2/SrRuO_3$ heterostructure grown on (001) $LaAlO_3$ that allows reversible modulation of the magnetization at room temperature (that imply both saturation magnetization and coercive field), possibly due to reorganization of the vacancy defects under the electric field influence.

5. Conclusions

Combining past and present studies, it can be observed that tremendous work has been put into determining the origin of d^0 magnetism in several structures. However, even though several strategies have been considered, there is still no clear understanding of the subject. Because they do not normally exhibit magnetic behavior, alkaline-earth hexaborides, non-magnetic oxides, and carbon nanostructures have been of great interest throughout the years due to their unexpected ferromagnetic behavior. The scientific community still debates the ability to induce magnetism in otherwise non-magnetic materials because it can open the path to a wide range of future applications.

Author Contributions: I.I.L., A.M.G. and C.F. participated in the review, writing, and revision. All authors have read and agreed to the published version of the manuscript.

Institutional Review Board Statement: Not applicable.

Informed Consent Statement: Not applicable.

Data Availability Statement: Not applicable.

Conflicts of Interest: The authors declare no conflict of interest.

References

1. Singh, R. Unexpected magnetism in nanomaterials. *J. Magn. Magn. Mater.* **2013**, *346*, 58–73. [CrossRef]
2. Makarova, T. Nanomagnetism in Otherwise Nonmagnetic Materials. *arXiv* **2009**; arXiv:0904.1550.
3. Coey, J.M.D.; Venkatesan, M.; Fitzgerald, C.B. Donor impurity band exchange in dilute ferromagnetic oxides. *Nat. Mater.* **2005**, *4*, 173–179. [CrossRef] [PubMed]
4. Das Sarma, S.; Hwang, E.H.; Kaminski, A. Temperature-dependent magnetization in diluted magnetic semiconductors. *Phys. Rev. B* **2003**, *67*, 155201. [CrossRef]
5. Kaminski, A.; Das Sarma, S. Polaron Percolation in Diluted Magnetic Semiconductors. *Phys. Rev. Lett.* **2002**, *88*, 247202. [CrossRef]
6. Coey, J.M.D.; Wongsaprom, K.; Alaria, J.; Venkatesan, M. Charge-transfer ferromagnetism in oxide nanoparticles. *J. Phys. D Appl. Phys.* **2008**, *41*, 134012. [CrossRef]
7. Dietl, T.; Haury, A.; Merle d'Aubigné, Y. Free carrier-induced ferromagnetism in structures of diluted magnetic semiconductors. *Phys. Rev. B* **1997**, *55*, R3347–R3350. [CrossRef]
8. Dietl, T.; Ohno, H.; Matsukura, F.; Cibert, J.; Ferrand, D. Zener Model Description of Ferromagnetism in Zinc-Blende Magnetic Semiconductors. *Science* **2000**, *287*, 1019. [CrossRef]
9. Dietl, T. Origin of ferromagnetic response in diluted magnetic semiconductors and oxides. *J. Phys. Condens. Matter* **2007**, *19*, 165204. [CrossRef]
10. Yokoyama, M.; Yamaguchi, H.; Ogawa, T.; Tanaka, M. Zinc-blende-type MnAs nanoclusters embedded in GaAs. *J. Appl. Phys.* **2005**, *97*, 10D317. [CrossRef]
11. Karczewski, G.; Sawicki, M.; Ivanov, V.; Ruester, C.; Grabecki, G.; Matsukura, F.; Molenkamp, L.W.; Dietl, T. Ferromagnetism in (Zn,Cr)Se Layers Grown by Molecular Beam Epitaxy. *J. Supercond.* **2003**, *16*, 55–58. [CrossRef]
12. Saito, H.; Zayets, V.; Yamagata, S.; Ando, K. Room-Temperature Ferromagnetism in a II-VI Diluted Magnetic Semiconductor Zn1−xCrxTe. *Phys. Rev. Lett.* **2003**, *90*, 207202. [CrossRef]

13. Cahill, J.T.; Graeve, O.A. Hexaborides: A review of structure, synthesis and processing. *J. Mater. Res. Technol.* **2019**, *8*, 6321–6335. [CrossRef]

14. Mohanta, S.K.; Mishra, S.N. Electronic structure and magnetic moment of dilute transition metal impurities in semi-metallic CaB6. *J. Magn. Magn. Mater.* **2017**, *444*, 349–353. [CrossRef]

15. Young, D.P.; Hall, D.; Torelli, M.E.; Fisk, Z.; Sarrao, J.L.; Thompson, J.D.; Ott, H.R.; Oseroff, S.B.; Goodrich, R.G.; Zysler, R. High-temperature weak ferromagnetism in a low-density free-electron gas. *Nature* **1999**, *397*, 412–414. [CrossRef]

16. Moriwaka, T.; Nishioka, T.; Sato Noriaki, K. Ferromagnetism Induced by Ca Vacancy in CaB 6. *J. Phys. Soc. Japan* **2001**, *70*, 341–344. [CrossRef]

17. Lofland, S.E.; Seaman, B.; Ramanujachary, K.V.; Hur, N.; Cheong, S.W. Defect driven magnetism in calcium hexaboride. *Phys. Rev. B* **2003**, *67*, 020410. [CrossRef]

18. Dorneles, L.S.; Venkatesan, M.; Moliner, M.; Lunney, J.G.; Coey, J.M.D. Magnetism in thin films of CaB6 and SrB6. *Appl. Phys. Lett.* **2004**, *85*, 6377–6379. [CrossRef]

19. Ackland, K.; Venkatesan, M.; Coey, J.M.D. Magnetism of BaB6 thin films synthesized by pulsed laser deposition. *J. Appl. Phys.* **2012**, *111*, 07A322. [CrossRef]

20. Bao, L.; Qi, X.; Tana; Chao, L.; Tegus, O. Synthesis, and magnetic and optical properties of nanocrystalline alkaline-earth hexaborides. *CrystEngComm* **2016**, *18*, 1223–1229. [CrossRef]

21. Koch, R.; Metz, P.C.; Jaime, O.; Vargas-Consuelos, C.I.; Borja-Urby, R.; Ko, J.Y.P.; Cahill, J.T.; Edwards, D.; Vasquez, V.R.; Graeve, O.A.; et al. Nanodomains and local structure in ternary alkaline-earth hexaborides. *J. Appl. Crystallogr.* **2018**, *51*, 1445–1454. [CrossRef]

22. Muñoz, M.C.; Gallego, S.; Sanchez, N. Surface ferromagnetism in non-magnetic and dilute magnetic oxides. *J. Phys. Conf. Ser.* **2011**, *303*, 012001. [CrossRef]

23. Yates, K. Dilute Magnetic Oxides: Current Status and Prospects. In *Nanomagnetism and Spintronics*; World Scientific: Singapore, 2010; pp. 223–265.

24. Venkatesan, M.; Fitzgerald, C.B.; Coey, J.M.D. Unexpected magnetism in a dielectric oxide. *Nature* **2004**, *430*, 630. [CrossRef] [PubMed]

25. Xie, Q.; Wang, W.-P.; Xie, Z.; Zhan, P.; Li, Z.-C.; Zhang, Z.-J. Room temperature ferromagnetism in un-doped amorphous HfO 2 nano-helix arrays. *Chin. Phys. B* **2015**, *24*, 057503. [CrossRef]

26. Zhang, Q.; Chen, G.; Yunoki, S. Surface ferromagnetism in HfO2 induced by excess oxygen. *Solid State Commun.* **2017**, *252*, 33–39. [CrossRef]

27. Singh, P.J.; Chae, H.K. d° Ferromagnetism of Magnesium Oxide. *Condens. Matter* **2017**, *2*, 36. [CrossRef]

28. Hassabo, A.G.; Mohamed, A.L. Novel flame retardant and antibacterial agent containing MgO NPs, phosphorus, nitrogen and silicon units for functionalise cotton fabrics. *Biointerface Res. Appl. Chem.* **2019**, *9*, 4272–4278. [CrossRef]

29. Droghetti, A.; Sanvito, S. Electron doping and magnetic moment formation in N- and C-doped MgO. *Appl. Phys. Lett.* **2009**, *94*, 252505. [CrossRef]

30. Araujo, C.M.; Kapilashrami, M.; Jun, X.; Jayakumar, O.D.; Nagar, S.; Wu, Y.; Århammar, C.; Johansson, B.; Belova, L.; Ahuja, R.; et al. Room temperature ferromagnetism in pristine MgO thin films. *Appl. Phys. Lett.* **2010**, *96*, 232505. [CrossRef]

31. Li, J.; Jiang, Y.; Li, Y.; Yang, D.; Xu, Y.; Yan, M. Origin of room temperature ferromagnetism in MgO films. *Appl. Phys. Lett.* **2013**, *102*, 072406. [CrossRef]

32. Mahadeva, S.K.; Fan, J.; Biswas, A.; Sreelatha, K.S.; Belova, L.; Rao, K.V. Magnetism of Amorphous and Nano-Crystallized Dc-Sputter-Deposited MgO Thin Films. *Nanomaterials* **2013**, *3*, 486–497. [CrossRef]

33. Wu, Y.; Yang, X.; Li, J.; Rao, K.V.; Belova, L. Solution processed room temperature ferromagnetic MgO thin films printed by inkjet technique. *Mater. Lett.* **2017**, *196*, 388–391. [CrossRef]

34. Khamkongkaeo, A.; Mothaneeyachart, N.; Sriwattana, P.; Boonchuduang, T.; Phetrattanarangsi, T.; Thongchai, C.; Sakkomolsri, B.; Pimsawat, A.; Daengsakul, S.; Phumying, S.; et al. Ferromagnetism and diamagnetism behaviors of MgO synthesized via thermal decomposition method. *J. Alloy. Compd.* **2017**, *705*, 668–674. [CrossRef]

35. Shojaee, A.; Mostafavi, A.; Shamspur, T.; Fathirad, F. Green synthesis of cerium oxide nanoparticles: Characterization, parameters optimization and investigation of photocatalytic application. *Biointerface Res. Appl. Chem.* **2020**, *10*, 5932–5937. [CrossRef]

36. Han, X.; Lee, J.; Yoo, H.-I. Oxygen-vacancy-induced ferromagnetism in CeO2 from first principles. *Phys. Rev. B* **2009**, *79*. [CrossRef]

37. Sundaresan, A.; Bhargavi, R.; Rangarajan, N.; Siddesh, U.; Rao, C.N.R. Ferromagnetism as a universal feature of nanoparticles of the otherwise non-magnetic oxides. *Phys. Rev. B* **2006**, *74*, 161306. [CrossRef]

38. Killivalavan, G.; Prabakar, A.C.; Naidu, K.C.B.; Sathyaseelan, B.; Rameshkumar, G.; Sivakumar, D.; Senthilnathan, K.; Baskaran, I.; Manikandan, E.; Rao, B.R. Synthesis and characterization of pure and Cu doped CeO2 nanoparticles: Photocatalytic and antibacterial activities evaluation. *Biointerface Res. Appl. Chem.* **2020**, *10*, 5306–5311. [CrossRef]

39. Liu, Y.; Lockman, Z.; Aziz, A.; MacManus-Driscoll, J. Size dependent ferromagnetism in cerium oxide (CeO2) nanostructures independent of oxygen vacancies. *J. Phys. Condens. Matter* **2008**, *20*, 165201. [CrossRef]

40. Fernandes, V.; Mossanek, R.J.O.; Schio, P.; Klein, J.J.; de Oliveira, A.J.A.; Ortiz, W.A.; Mattoso, N.; Varalda, J.; Schreiner, W.H.; Abbate, M.; et al. Dilute-defect magnetism: Origin of magnetism in nanocrystalline CeO$_2$. *Phys. Rev. B* **2009**, *80*, 035202. [CrossRef]

41. Ribeiro, A.; Ferreira, N. Systematic study of the physical origin of ferromagnetism in CeO 2−δ nanoparticles. *Phys. Rev. B* **2017**, *95*. [CrossRef]

42. Paidi, V.K.; Brewe, D.L.; Freeland, J.W.; Roberts, C.A.; van Lierop, J. Role of Ce $4f$ hybridization in the origin of magnetism in nanoceria. *Phys. Rev. B* **2019**, *99*, 180403. [CrossRef]

43. Varalda, J.; Dartora, C.A.; de Camargo, P.C.; de Oliveira, A.J.A.; Mosca, D.H. Oxygen diffusion and vacancy migration thermally-activated govern high-temperature magnetism in ceria. *Sci. Rep.* **2019**, *9*, 4708. [CrossRef] [PubMed]

44. Straumal, B.B.; Protasova, S.G.; Mazilkin, A.A.; Goering, E.; Schütz, G.; Straumal, P.B.; Baretzky, B. Ferromagnetic behaviour of ZnO: The role of grain boundaries. *Beilstein J. Nanotechnol.* **2016**, *7*, 1936–1947. [CrossRef] [PubMed]

45. Sato, K.; Katayama-Yoshida, H. First principles materials design for semiconductor spintronics. *Semicond. Sci. Technol.* **2002**, *17*, 367–376. [CrossRef]

46. Droepenu, E.K.; Wee, B.S.; Chin, S.F.; Kok, K.Y.; Asare, E.A. Synthesis and characterization of single phase ZnO nanostructures via solvothermal method: Influence of alkaline source. *Biointerface Res. Appl. Chem.* **2020**, *10*, 5648–5655. [CrossRef]

47. Lin, X.-L.; Yan, S.-S.; Zhao, M.-W.; Hu, S.-J.; Han, C.; Chen, Y.-X.; Liu, G.-L.; Dai, Y.-Y.; Mei, L.-M. Possible origin of ferromagnetism in un-doped ZnO: First-principles calculations. *Phys. Lett. A* **2011**, *375*, 638–641. [CrossRef]

48. Wu, H.; Stroppa, A.; Sakong, S.; Picozzi, S.; Scheffler, M.; Kratzer, P. Magnetism in C- or N-doped MgO and ZnO: A Density-Functional Study of Impurity Pairs. *Phys. Rev. Lett.* **2010**, *105*, 267203. [CrossRef]

49. Straumal, B.B.; Mazilkin, A.A.; Protasova, S.G.; Myatiev, A.A.; Straumal, P.B.; Schütz, G.; van Aken, P.A.; Goering, E.; Baretzky, B. Magnetization study of nanograined pure and Mn-doped ZnO films: Formation of a ferromagnetic grain-boundary foam. *Phys. Rev. B* **2009**, *79*, 205206. [CrossRef]

50. Pazhanivelu, D.V.; Blessington, P.; Rathinasamy, M. Unexpected ferromagnetism in Ist group elements doped ZnO based DMS nanoparticles. *Mater. Lett.* **2015**, *151*. [CrossRef]

51. Gao, D.; Zhang, Z.; Fu, J.; Xu, Y.; Qi, J.; Xue, D. Room temperature ferromagnetism of pure ZnO nanoparticles. *J. Appl. Phys.* **2009**, *105*, 113928. [CrossRef]

52. Sun, Y.; Zong, Y.; Feng, J.; Li, X.; Yan, F.; Lan, Y.; Zhang, L.; Ren, Z.; Zheng, X. Oxygen vacancies driven size-dependent d0 room temperature ferromagnetism in well-dispersed dopant-free ZnO nanoparticles and density functional theory calculation. *J. Alloy. Compd.* **2018**, *739*, 1080–1088. [CrossRef]

53. Wang, Y.; Huang, Y.; Song, Y.; Zhang, X.; Ma, Y.; Liang, J.; Chen, Y. Room-Temperature Ferromagnetism of Graphene. *Nano Lett.* **2009**, *9*, 220–224. [CrossRef] [PubMed]

54. Stamenov, P.; Coey, J.M.D. Magnetic susceptibility of carbon—Experiment and theory. *J. Magn. Magn. Mater.* **2005**, *290–291*, 279–285. [CrossRef]

55. Kroto, H.W.; Heath, J.R.; O'Brien, S.C.; Curl, R.F.; Smalley, R.E. C60: Buckminsterfullerene. *Nature* **1985**, *318*, 162–163. [CrossRef]

56. Höhne, R.; Esquinazi, P. Can Carbon Be Ferromagnetic? *Adv. Mater.* **2002**, *14*, 753–756. [CrossRef]

57. Ata, M.; Machida, M.; Watanabe, H.; Seto, J.e. Polymer-C60Composite with Ferromagnetism. *Jpn. J. Appl. Phys.* **1994**, *33*, 1865–1871. [CrossRef]

58. Makarova, T.L.; Sundqvist, B. Pressure-induced ferromagnetism of fullerenes. *High. Press. Res.* **2003**, *23*, 135–141. [CrossRef]

59. Makarova, T. Magnetism in Polymerized Fullerenes. In *Frontiers of Multifunctional Integrated Nanosystems*; Springer: Dordrecht, The Netherlands, 2005; Volume 152, p. 331.

60. Wood, R.A.; Lewis, M.H.; Lees, M.R.; Bennington, S.M.; Cain, M.G.; Kitamura, N. Ferromagnetic fullerene. *J. Phys. Condens. Matter* **2002**, *14*, L385–L391. [CrossRef]

61. Murakami, Y.; Suematsu, H. Magnetism of C60 induced by photo-assisted oxidation. *Pure Appl. Chem.* **1996**, *68*, 1463–1467. [CrossRef]

62. Ghosh, S.; Tongay, S.; Hebard, A.F.; Sahin, H.; Peeters, F.M. Ferromagnetism in stacked bilayers of Pd/C60. *J. Magn. Magn. Mater.* **2014**, *349*, 128–134. [CrossRef]

63. Vozmediano, M.A.H.; López-Sancho, M.P.; Stauber, T.; Guinea, F. Local defects and ferromagnetism in graphene layers. *Phys. Rev. B* **2005**, *72*, 155121. [CrossRef]

64. Yazyev, O.V.; Helm, L. Defect-induced magnetism in graphene. *Phys. Rev. B* **2007**, *75*, 125408. [CrossRef]

65. Radovic, L.R.; Bockrath, B. On the Chemical Nature of Graphene Edges: Origin of Stability and Potential for Magnetism in Carbon Materials. *J. Am. Chem. Soc.* **2005**, *127*, 5917–5927. [CrossRef]

66. Wang, W.L.; Meng, S.; Kaxiras, E. Graphene NanoFlakes with Large Spin. *Nano Letters* **2008**, *8*, 241–245. [CrossRef]

67. Sahu, V.; Maurya, V.K.; Singh, G.; Patnaik, S.; Sharma, R.K. Enhanced ferromagnetism in edge enriched holey/lacey reduced graphene oxide nanoribbons. *Mater. Design* **2017**, *132*, 295–301. [CrossRef]

68. Sharpe, A.L.; Fox, E.J.; Barnard, A.W.; Finney, J.; Watanabe, K.; Taniguchi, T.; Kastner, M.A.; Goldhaber-Gordon, D. Emergent ferromagnetism near three-quarters filling in twisted bilayer graphene. *Science* **2019**, *365*, 605. [CrossRef] [PubMed]

69. Tuček, J.; Holá, K.; Zoppellaro, G.; Błoński, P.; Langer, R.; Medved', M.; Susi, T.; Otyepka, M.; Zbořil, R. Zigzag sp2 Carbon Chains Passing through an sp3 Framework: A Driving Force toward Room-Temperature Ferromagnetic Graphene. *ACS Nano* **2018**, *12*, 12847–12859. [CrossRef] [PubMed]

70. Badry, R.; Radwan, S.H.; Ezzat, D.; Ezzat, H.; Elhaes, H.; Ibrahim, M. Study of the Electronic Properties of Graphene Oxide/(PANi/Teflon). *Biointerface Res. Appl. Chem.* **2020**, *10*, 6926–6935. [CrossRef]

71. Daoudi, K.; Gaidi, M.; Columbus, S. Silver nanoprisms/graphene oxide/silicon nanowires composites for R6G surface-enhanced Raman spectroscopy sensor. *Biointerface Res. Appl. Chem.* **2020**, *10*, 5670–5674. [CrossRef]

72. Sun, X.L.; Qi, Z.; Li, Q.Q.; Zhang, X.R.; Shao, X.L.; Jin, Y.; Zhang, J.J.; Liu, Y.Y. Utilization of carbon nanotube and graphene in electrochemical CO2 reduction. *Biointerface Res. Appl. Chem.* **2020**, *10*, 5815–5827. [CrossRef]

73. Swamy, B.K.; Shiprath, K.; Rakesh, G.; Ratnam, K.V.; Manjunatha, H.; Janardan, S.; Naidu, K.C.B.; Ramesh, S.; Suresh, K.; Ratnamala, A. Simultaneous detection of dopamine, tyrosine and ascorbic acid using NiO/graphene modified graphite electrode. *Biointerface Res. Appl. Chem.* **2020**, *10*, 5599–5609. [CrossRef]

74. Lehtinen, P.O.; Foster, A.S.; Ma, Y.; Krasheninnikov, A.V.; Nieminen, R.M. Irradiation-induced magnetism in graphite: A density functional study. *Phys. Rev. Lett.* **2004**, *93*, 187202. [CrossRef] [PubMed]

75. Mombrú, A.; Pardo, H.; Faccio, R.; Lima, O.; Leite, E.; Zanelatto, G.; Lanfredi, A.; Cardoso, C.; Araujo-Moreira, F. Multilevel ferromagnetic behavior of room-temperature bulk magnetic graphite. *Phys. Rev. B* **2005**, *71*. [CrossRef]

76. Esquinazi, P.; Setzer, A.; Höhne, R.; Semmelhack, C.; Kopelevich, Y.; Spemann, D.; Butz, T.; Kohlstrunk, B.; Lösche, M. Ferromagnetism in oriented graphite samples. *Phys. Rev. B* **2002**, *66*, 024429. [CrossRef]

77. He, Z.; Xia, H.; Zhou, X.; Yang, X.; Wang, T. Raman study of correlation between defects and ferromagnetism in graphite. *J. Phys. D Appl. Phys.* **2011**, *44*, 085001. [CrossRef]

78. Yang, X.; Xia, H.; Qin, X.; Li, W.; Dai, Y.; Liu, X.; Zhao, M.; Xia, Y.; Yan, S.; Wang, B. Correlation between the vacancy defects and ferromagnetism in graphite. *Carbon* **2009**, *47*, 1399–1406. [CrossRef]

79. Guevenilir, E.; Kincal, C.; Kamber, U.; Guerlue, O.; Yildiz, D.; Grygiel, C.; Van der Beek, C.J. Investigation of ferromagnetism on graphite due to swift heavy ion irradiation. In *Verhandlungen der Deutschen Physikalischen Gesellschaft*; International Atomic Energy Agency (IAEA): Dresden, Germany, 2017; Volume 1.

80. Haroun, A.A.; Ahmed, H.M.; Mossa, A.T.H.; Mohafrash, S.M.; Ahmed, E.F. Production, characterization and immobilization of Aspergillus versicolor L-asparaginase onto multi-walled carbon nanotubes. *Biointerface Res. Appl. Chem.* **2020**, *10*, 5733–5740. [CrossRef]

81. Céspedes, O.; Ferreira, M.S.; Sanvito, S.; Kociak, M.; Coey, J.M.D. Contact induced magnetism in carbon nanotubes. *J. Phys. Condens. Matter* **2004**, *16*, L155–L161. [CrossRef]

82. Friedman, A.L.; Chun, H.; Jung, Y.J.; Heiman, D.; Glaser, E.R.; Menon, L. Possible room-temperature ferromagnetism in hydrogenated carbon nanotubes. *Phys. Rev. B* **2010**, *81*, 115461. [CrossRef]

83. Fang, Z.; Zhao, H.; Xiong, L.; Zhang, F.; Fu, Q.; Ma, Z.; Xu, C.; Lin, Z.; Wang, H.; Hu, Z.; et al. Enhanced ferromagnetic properties of N2 plasma-treated carbon nanotubes. *J. Mater. Sci.* **2019**, *54*, 2307–2314. [CrossRef]

84. Kim, D.W.; Lee, K.W.; Lee, C.E. Defect-induced room-temperature ferromagnetism in single-walled carbon nanotubes. *J. Magn. Magn. Mater.* **2018**, *460*, 397–400. [CrossRef]

85. Singh, S.B.; Wang, Y.-F.; Shao, Y.-C.; Lai, H.-Y.; Hsieh, S.-H.; Limaye, M.V.; Chuang, C.-H.; Hsueh, H.-C.; Wang, H.; Chiou, J.-W.; et al. Observation of the origin of d0 magnetism in ZnO nanostructures using X-ray-based microscopic and spectroscopic techniques. *Nanoscale* **2014**, *6*, 9166–9176. [CrossRef] [PubMed]

86. Chaboy, J.; Boada, R.; Piquer, C.; Laguna-Marco, M.A.; García-Hernández, M.; Carmona, N.; Llopis, J.; Ruíz-González, M.L.; González-Calbet, J.; Fernández, J.F.; et al. Evidence of intrinsic magnetism in capped ZnO nanoparticles. *Phys. Rev. B* **2010**, *82*, 064411. [CrossRef]

87. Zippel, J.; Lorenz, M.; Setzer, A.; Wagner, G.; Sobolev, N.; Esquinazi, P.; Grundmann, M. Defect-induced ferromagnetism in undoped and Mn-doped zirconia thin films. *Phys. Rev. B* **2010**, *82*, 125209. [CrossRef]

88. Zhan, P.; Xie, Z.; Li, Z.; Wang, W.; Zhang, Z.; Li, Z.; Cheng, G.; Zhang, P.; Wang, B.; Cao, X. Origin of the defects-induced ferromagnetism in un-doped ZnO single crystals. *Appl. Phys. Lett.* **2013**, *102*, 071914. [CrossRef]

89. Liu, Y.; Zhou, W.; Huang, Y.; Wu, P. Unexpected ferromagnetism in n-type polycrystalline K-doped ZnO films prepared by RF-magnetron sputtering. *J. Mater. Sci. Mater. Electron.* **2015**, *26*, 8451–8455. [CrossRef]

90. Naji Aljawfi, R.; Rahman, F.; Shukla, D.K. Effect of the annealing temperature on the structural and magnetic properties of ZnO nanoparticles. *Mater. Lett.* **2013**, *99*, 18–20. [CrossRef]

91. Zhan, P.; Wang, W.; Liu, C.; Hu, Y.; Li, Z.; Zhang, Z.; Zhang, P.; Wang, B.; Cao, X. Oxygen vacancy–induced ferromagnetism in un-doped ZnO thin films. *J. Appl. Phys.* **2012**, *111*, 033501. [CrossRef]

92. Phan, T.-L.; Zhang, Y.D.; Yang, D.S.; Nghia, N.X.; Thanh, T.D.; Yu, S.C. Defect-induced ferromagnetism in ZnO nanoparticles prepared by mechanical milling. *Appl. Phys. Lett.* **2013**, *102*, 072408. [CrossRef]

93. Das, J.; Pradhan, S.K.; Mishra, D.K.; Sahu, D.R.; Sarangi, S.; Varma, S.; Nayak, B.B.; Huang, J.-L.; Roul, B.K. Unusual ferromagnetism in high purity ZnO sintered ceramics. *Mater. Res. Bull.* **2011**, *46*, 42–47. [CrossRef]

94. Poornaprakash, B.; Chalapathi, U.; Babu, S.; Park, S.-H. Structural, morphological, optical, and magnetic properties of Gd-doped and (Gd, Mn) co-doped ZnO nanoparticles. *Phys. E Low-Dimens. Syst. Nanostructures* **2017**, *93*, 111–115. [CrossRef]

95. Zhu, M.; Zhang, Z.; Zhong, M.; Tariq, M.; Li, Y.; Li, W.; Jin, H.; Skotnicova, K.; Li, Y. Oxygen vacancy induced ferromagnetism in Cu-doped ZnO. *Ceram. Int.* **2016**, *43*. [CrossRef]

96. Rumaiz, A.K.; Ali, B.; Ceylan, A.; Boggs, M.; Beebe, T.; Ismat Shah, S. Experimental studies on vacancy induced ferromagnetism in undoped TiO2. *Solid State Commun.* **2007**, *144*, 334–338. [CrossRef]

97. Kim, D.; Hong, J.; Park, Y.R.; Kim, K.J. The origin of oxygen vacancy induced ferromagnetism in undoped TiO2. *J. Phys. Condens. Matter* **2009**, *21*, 195405. [CrossRef] [PubMed]

98. Singhal, R.K.; Kumar, S.; Kumari, P.; Xing, Y.T.; Saitovitch, E. Evidence of defect-induced ferromagnetism and its "switch" action in pristine bulk TiO2. *Appl. Phys. Lett.* **2011**, *98*, 092510. [CrossRef]

99. Sangaletti, L.; Mozzati, M.C.; Galinetto, P.; Azzoni, C.B.; Speghini, A.; Bettinelli, M.; Calestani, G. Ferromagnetism on a paramagnetic host background: The case of rutile TM:TiO2single crystals (TM = Cr, Mn, Fe, Co, Ni, Cu). *J. Phys. Condens. Matter* **2006**, *18*, 7643–7650. [CrossRef] [PubMed]

100. Singhal, R.K.; Samariya, A.; Kumar, S.; Xing, Y.T.; Jain, D.C.; Dolia, S.N.; Deshpande, U.P.; Shripathi, T.; Saitovitch, E.B. Study of defect-induced ferromagnetism in hydrogenated anatase TiO2:Co. *J. Appl. Phys.* **2010**, *107*, 113916. [CrossRef]

101. Potzger, K.; Osten, J.; Levin, A.A.; Shalimov, A.; Talut, G.; Reuther, H.; Arpaci, S.; Bürger, D.; Schmidt, H.; Nestler, T.; et al. Defect-induced ferromagnetism in crystalline SrTiO3. *J. Magn. Magn. Mater.* **2011**, *323*, 1551–1562. [CrossRef]

102. Shi, S.; Gao, D.; Xu, Q.; Yang, Z.; Xue, D. Singly-charged oxygen vacancy-induced ferromagnetism in mechanically milled SnO2 powders. *RSC Adv.* **2014**, *4*, 45467–45472. [CrossRef]

103. Mehraj, S.; Ansari, M.S.; Al-Ghamdi, A.A.; Alimuddin. Annealing dependent oxygen vacancies in SnO2 nanoparticles: Structural, electrical and their ferromagnetic behavior. *Mater. Chem. Phys.* **2016**, *171*, 109–118. [CrossRef]

104. Chang, G.S.; Forrest, J.; Kurmaev, E.Z.; Morozovska, A.N.; Glinchuk, M.D.; McLeod, J.A.; Moewes, A.; Surkova, T.P.; Hong, N.H. Oxygen-vacancy-induced ferromagnetism in undoped SnO_2 thin films. *Phys. Rev. B* **2012**, *85*, 165319. [CrossRef]

105. Lee, Y.F.; Wu, F.; Kumar, R.; Hunte, F.; Schwartz, J.; Narayan, J. Epitaxial integration of dilute magnetic semiconductor Sr3SnO with Si (001). *Appl. Phys. Lett.* **2013**, *103*, 112101. [CrossRef]

106. Qi, L.-Q.; Han, R.-S.; Liu, L.-H.; Sun, H.-Y. Preparation and magnetic properties of DC-sputtered porous HfO2 films. *Ceram. Int.* **2016**, *42*, 18925–18930. [CrossRef]

107. Zhao, G.; Zhang, L.; Hu, L.; Yu, H.; Min, G.; Yu, H. Structure and magnetic properties of nanocrystalline CaB6 films deposited by magnetron sputtering. *J. Alloy. Compd.* **2014**, *599*, 175–178. [CrossRef]

108. Bennett, M.C.; van Lierop, J.; Berkeley, E.M.; Mansfield, J.F.; Henderson, C.; Aronson, M.C.; Young, D.P.; Bianchi, A.; Fisk, Z.; Balakirev, F.; et al. Weak ferromagnetism in CaB6. *Phys. Rev. B* **2004**, *69*, 132407. [CrossRef]

109. Coey, J.M.D. Publisher Correction: Magnetism in d0 oxides. *Nat. Mater.* **2019**, *18*, 770. [CrossRef] [PubMed]

110. Simões Valentin, C.B.; de Sousa e Silva, R.L.; Banerjee, P.; Franco, A. Investigation of Fe-doped room temperature dilute magnetic ZnO semiconductors. *Mater. Sci. Semicond. Process.* **2019**, *96*, 122–126. [CrossRef]

111. Elilarassi, R.; Chandrasekaran, G. Optical, electrical and ferromagnetic studies of ZnO:Fe diluted magnetic semiconductor nanoparticles for spintronic applications. *Spectrochim. Acta Part. A Mol. Biomol. Spectrosc.* **2017**, *186*, 120–131. [CrossRef]

112. Mantovan, R.; Gunnlaugsson, H.P.; Johnston, K.; Masenda, H.; Mølholt, T.E.; Naidoo, D.; Ncube, M.; Shayestehaminzadeh, S.; Bharuth-Ram, K.; Fanciulli, M.; et al. Atomic-Scale Magnetic Properties of Truly 3d-Diluted ZnO. *Adv. Electron. Mater.* **2015**, *1*, 1400039. [CrossRef]

113. Qi, B.; Ólafsson, S.; Gíslason, H.P. Vacancy defect-induced d0 ferromagnetism in undoped ZnO nanostructures: Controversial origin and challenges. *Prog. Mater. Sci.* **2017**, *90*, 45–74. [CrossRef]

114. Garcia, M.A.; Fernandez Pinel, E.; de la Venta, J.; Quesada, A.; Bouzas, V.; Fernández, J.F.; Romero, J.J.; Martín González, M.S.; Costa-Krämer, J.L. Sources of experimental errors in the observation of nanoscale magnetism. *J. Appl. Phys.* **2009**, *105*, 013925. [CrossRef]

115. Pereira, L.M.C. Experimentally evaluating the origin of dilute magnetism in nanomaterials. *J. Phys. D Appl. Phys.* **2017**, *50*, 393002. [CrossRef]

116. Song, C.; Pan, F. Chapter Seven—Transition Metal-Doped Magnetic Oxides. In *Semiconductors and Semimetals*; Svensson, B.G., Pearton, S.J., Jagadish, C., Eds.; Elsevier: Amsterdam, The Netherlands, 2013; Volume 88, pp. 227–259.

117. Wolf, S.A.; Chtchelkanova, A.Y.; Treger, D.M. Spintronics—A retrospective and perspective. *IBM J. Res. Dev.* **2006**, *50*, 101–110. [CrossRef]

118. Sinova, J.; Žutić, I. New moves of the spintronics tango. *Nat. Mater.* **2012**, *11*, 368–371. [CrossRef]

119. Wolf, S.A.; Awschalom, D.D.; Buhrman, R.A.; Daughton, J.M.; von Molnár, S.; Roukes, M.L.; Chtchelkanova, A.Y.; Treger, D.M. Spintronics: A Spin-Based Electronics Vision for the Future. *Science* **2001**, *294*, 1488. [CrossRef]

120. Pan, F.; Song, C.; Liu, X.J.; Yang, Y.C.; Zeng, F. Ferromagnetism and possible application in spintronics of transition-metal-doped ZnO films. *Mater. Sci. Eng. R Rep.* **2008**, *62*, 1–35. [CrossRef]

121. Zhu, J.-G.; Park, C. Magnetic tunnel junctions. *Mater. Today* **2006**, *9*, 36–45. [CrossRef]

122. Toyosaki, H.; Fukumura, T.; Ueno, K.; Nakano, M.; Kawasaki, M. A Ferromagnetic Oxide Semiconductor as Spin Injection Electrode in Magnetic Tunnel Junction. *Jpn. J. Appl. Phys.* **2005**, *44*, L896–L898. [CrossRef]

123. Liu, X.; Zeng, F.; Pan, F. Fully epitaxial (Zn,Co)O/ZnO/(Zn,Co)O junction and its tunnel magnetoresistance. *Appl. Phys. Lett.* **2007**, *91*, 042106. [CrossRef]

124. Ohno, H.; Chiba, D.; Matsukura, F.; Omiya, T.; Abe, E.; Dietl, T.; Ohno, Y.; Ohtani, K. Electric-field control of ferromagnetism. *Nature* **2000**, *408*, 944–946. [CrossRef] [PubMed]

125. Chiba, D.; Sawicki, M.; Nishitani, Y.; Nakatani, Y.; Matsukura, F.; Ohno, H. Magnetization vector manipulation by electric fields. *Nature* **2008**, *455*, 515–518. [CrossRef] [PubMed]

126. Zhao, T.; Shinde, S.R.; Ogale, S.B.; Zheng, H.; Venkatesan, T.; Ramesh, R.; Das Sarma, S. Electric field effect in diluted magnetic insulator anatase Co: TiO2. *Phys. Rev. Lett.* **2005**, *94*, 126601. [CrossRef] [PubMed]